NASA SP-289

# APOLLO 15

# Preliminary Science Report

PREPARED BY

NASA MANNED SPACECRAFT CENTER

*Scientific and Technical Information Office* 1972

NATIONAL AERONAUTICS AND SPACE ADMINISTRATION

*Washington, D.C.*

# 11. Heat-Flow Experiment

*Marcus G. Langseth, Jr.,*[a†] *Sydney P. Clark, Jr.,*[b] *John L. Chute, Jr.,*[a]
*Stephen J. Keihm,*[a] *and Alfred E. Wechsler*[c]

The purpose of the heat-flow experiment is to determine the rate of heat flow from the lunar interior by temperature and thermal-property measurements in the lunar subsurface. Heat loss is directly related to the internal temperature and the rate of internal heat production; therefore, measurements of these quantities enable limits to be set on long-lived radioisotopic abundances (the chief source of interior heating), the internal temperature, and the thermal evolution of the Moon.

Preliminary analysis of the data from one heat-flow probe indicates that the heat flow from depth below the Hadley Rille site is $3.3 \times 10^{-6}$ W/cm$^2$ (±15 percent). This value is approximately one-half the average heat flow of the Earth. Further analysis of data over several lunations is required to demonstrate that this value is representative of the heat flow at the Hadley Rille site. Subsurface temperature at a depth of 1 m below the surface is approximately 252.4 K at one probe site and 250.7 K at the other site. These temperatures are approximately 35 K above the mean surface temperature and indicate that the thermal conductivity in the surficial layer of the Moon is highly temperature dependent. Between 1 and 1.5 m, the rate of temperature increase as a function of depth is 1.75 K/m (±2 percent) at the probe 1 site. In situ measurements indicate that the thermal conductivity of the regolith increases with depth. Thermal-conductivity values between $1.4 \times 10^{-4}$ and $2.5 \times 10^{-4}$ W/cm-K were determined; these values are a factor of 7 to 10 greater than the values of the surface conductivity. Lunar-surface brightness temperatures during the first lunar night have been deduced from temperatures of thermocouples above and on the lunar surface. The cooldown history after sunset suggests that a substantial increase in conductivity occurs at a depth on the order of several centimeters. Temperature measurements were also recorded during the total eclipse on August 6, 1971.

[a]Lamont-Doherty Geological Observatory.
[b]Yale University.
[c]Arthur D. Little, Inc.
†Principal investigator.

## EXPERIMENT CONCEPT AND DESIGN

### Heat Budget in the Surface Layer of the Moon

The temperature and the heat flux at the surface of the Moon are determined mainly by the solar energy impinging on the surface during one-half of the 29.5-day lunation cycle. During the lunar day, the surface temperature rises to approximately 380 K, which results in heat flow into the subsurface. After lunar sunset, the surface temperature drops to nearly 100 K, and heat flows out of the subsurface and is lost by radiation into space. These very large temperature excursions, in part, are a result of the extremely low thermal conductivity and volumetric heat capacity of the fine rock powders that mantle most of the lunar surface (ref. 11-1) and, in part, are a result of the very tenuous atmosphere of the Moon. The low thermal conductivity of the bulk of the regolith (ref. 11-2) strongly inhibits the flow of energy into and out of the subsurface. At a depth of approximately 50 cm, the large surface variation of 280 K is attenuated to a nearly undetectable amplitude.

At low lunar latitudes, the surface temperature, averaged over one lunation, is approximately 220 K. This mean surface temperature is determined by the balance of solar energy flowing into and energy radiated out of the surface during a complete lunation. The mean temperature in the subsurface (at decimeter depths) may be higher than the mean

surface temperature by a few tens of degrees. As will be shown in more detail later in this section, the mean subsurface temperature at the Hadley Rille site is considerably higher than the mean surface temperature. This increase in mean temperature is a result of the important role of heat transfer by radiation in the fine powders on the surface. The efficiency of radiative heat transfer between particles varies in proportion to the cube of the absolute temperature (ref. 11-3); consequently, during the lunar day, heat flows more readily into the Moon than it flows out during the night. The subsurface heat balance, over one lunation, requires that a substantial steady-state heat loss be maintained in the upper several centimeters of lunar material to eliminate the excess heat that penetrates during the day (ref. 11-4). This outward heat flow causes a steep downward increase in mean temperature that extends to a depth of a few decimeters, the depth to which diurnal waves penetrate.

At depths greater than those to which diurnal waves penetrate, the thermal regime is dominated by heat flow from the lunar interior. This flow results from high interior temperatures and, in the subsurface, is directly proportional to the increase of temperature with depth (the vertical temperature gradient) and to the thermal conductivity. These quantities are related by the equation

$$F_z = -k \frac{dT}{dz} \qquad (11\text{-}1)$$

where $F_z$ is the vertical component of the heat flow, $k$ is the thermal conductivity, $T$ is the temperature, and $z$ is the depth. The average heat flow of the Earth has been determined to be $6.2 \times 10^{-6}$ W/cm$^2$ by numerous measurements (ref. 11-5). Estimates of the lunar heat flow, based on microwave emission from the Moon, have ranged from $1.0 \times 10^{-6}$ W/cm$^2$ (ref. 11-6) to $3.3 \times 10^{-6}$ W/cm$^2$ (ref. 11-7), or one-sixth to one-half the Earth heat flow. Thermal-history calculations, based on chrondritic- and terrestrial-isotope abundances for the Moon (ref. 11-8), result in heat-flow estimates of $1 \times 10^{-6}$ to $2.5 \times 10^{-6}$ W/cm$^2$ for this period in the lunar history. Because of the extremely low conductivity of the regolith, even these very low heat flows would result in gradients ranging from a few tenths of a degree per meter to a few degrees per meter.

## Instrument Design

The essential measurements for determining heat flow are made by two slender temperature-sensing probes that are placed in predrilled holes in the subsurface, spaced approximately 10 m apart. Two probes enable two independent measurements of the heat flow to be made in order to gain some knowledge of the lateral variation of heat flow at the Hadley Rille site. Each probe consists of two nearly identical 50-cm-long sections (fig. 11-1). Each section of each heat-flow probe has two accurate (±0.001 K) differential thermometers that measure temperature differences between points separated by approximately 47 and 28 cm. With these thermometers, a measurement (with an accuracy of ±0.05 K) of absolute temperature at four points on each probe section also can be made.

Additional temperature measurements are provided by four thermocouple junctions in the cables that connect each probe to the electronics unit. The thermocouple junctions are located at distances of approximately 0, 0.65, 1.15, and 1.65 m from the topmost gradient sensors (fig. 11-1). The reference junction for these thermocouples is thermally joined to a platinum-resistance reference thermometer, which is mounted on the radiator plate of the electronics unit. The temperature measurements obtained from the heat-flow experiment are summarized in table 11-I.

The differential thermometers consist of four platinum resistance elements wired in a bridge configuration (fig. 11-2). The bridge is excited by successive 2.6-msec, 8-V pulses, first of one polarity and then of the other. The output voltage, the excitation voltage, and the bridge current are measured and used to determine the absolute temperature and the temperature difference. The ratio of bridge output voltage to excitation voltage and the bridge resistance are calibrated for 42 different pairs of temperature and temperature-difference values. The accuracy of these calibrations is better than the accuracies specified in table 11-I. The thermocouples are calibrated at four temperature points, and the reference bridge is calibrated at five temperature points.

Conductivity measurements are made by means of heaters that surround each of the eight gradient-bridge sensors. The experiment is designed to measure conductivity in two ranges: a lower range of $1 \times$

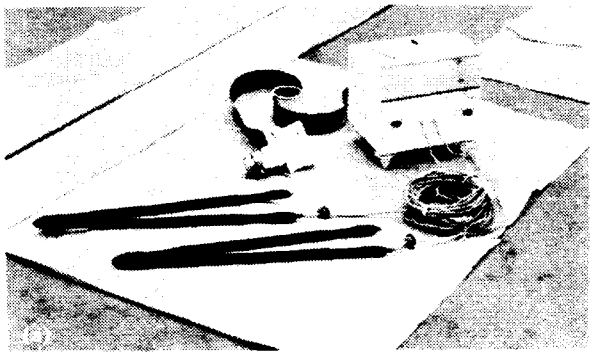

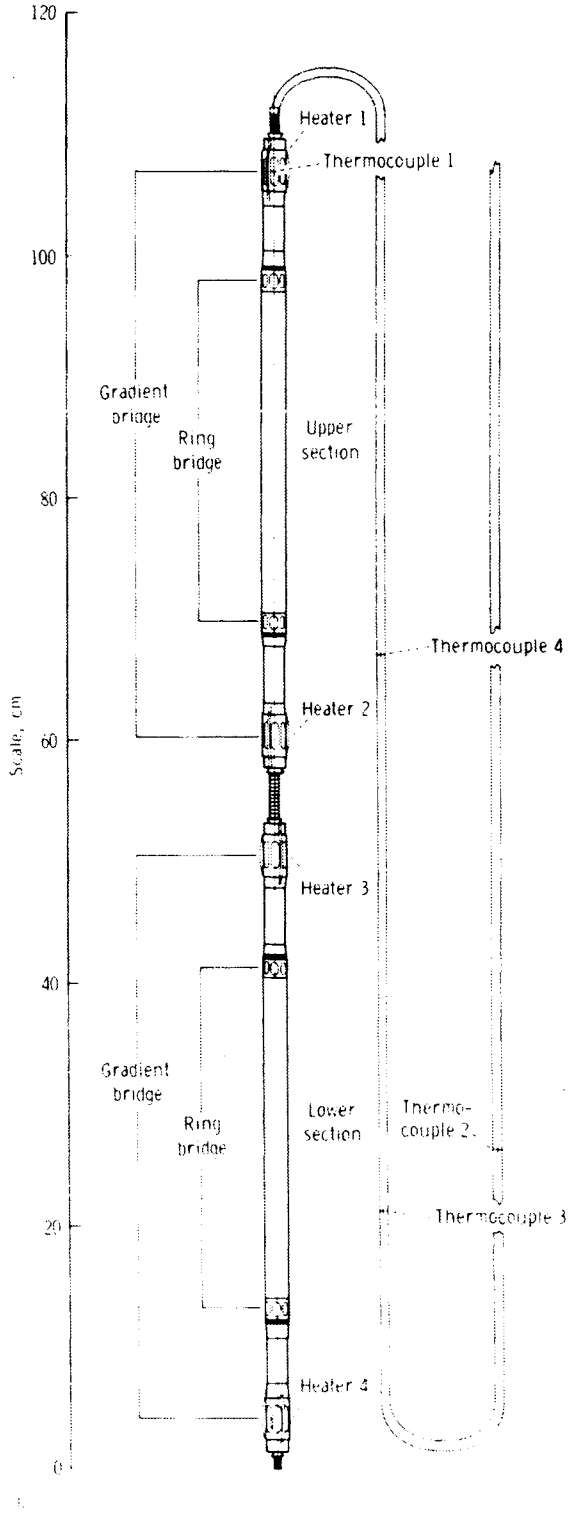


FIGURE 11-1.–Heat-flow experiment and dual-purpose heat-flow probe. (a) Heat-flow-experiment equipment. (b) Schematic of heat-flow probe.

$10^{-5}$ to $5 \times 10^{-4}$ W/cm-K and a higher range of $2 \times 10^{-4}$ to $4 \times 10^{-3}$ W/cm-K. To enable measurements in the lower range to be made, a heater is energized at 0.002 W, and the temperature rise of the underlying gradient sensor is recorded as a function of time for a period of 36 hr. The temperature rise and the rate of temperature rise can be interpreted in terms of the conductivity of the surrounding lunar material. Measurements in the higher range of conductivities are made by energizing the same heater at 0.5 W and monitoring the temperature rise at the ring sensor 10 cm away for a period of approximately 8 hr.

## Operation of the Experiment

During normal operation of the experiment (mode 1 operation), temperatures of all gradient bridges, thermocouples, and the reference bridge (as well as temperature differences of all gradient bridges) are sampled every 7.2 min. When a heater is turned on at 0.002 W to enable measurements to be made in the lower conductivity range, the experiment is said to be operating in mode 2. The mode 3 operation is designed for the measurement of conductivity in the higher range. In this mode, temperature and temperature difference at a selected ring bridge are read every 54 sec. These modes of operation and heater turnon are controlled by commands transmitted from Earth.

The detection circuitry for measuring bridge voltages and thermocouple outputs is contained in a housing separate from the Apollo lunar surface experiments package (ALSEP) central station (fig. 11-1(a)) and is designed to compensate for amplifier offset and gain change. This compensation is achieved

TABLE 11-I.–*Summary of the Heat-Flow-Experiment Temperature Measurements*

| *Thermometer* | *Number* | *Location* | *Temperature difference, K* | | *Absolute temperature, K* | |
|---|---|---|---|---|---|---|
| | | | *Range* | *Accuracy* | *Range* | *Accuracy* |
| Gradient bridge[a] | 1 per section | Sensors separated by 47 cm | ±2<br>±20 | ±0.001<br>±0.01 | 190 to 270 | ±0.05 |
| Ring bridge | 1 per section | Sensors separated by 28 cm | ±2 | ±0.002 | 190 to 270 | ±0.05 |
| Thermocouple | 4 per probe | Spaced 65 cm apart in the first 2.5 m of the cable above the probe | -- | -- | 70 to 400 | ±0.07 |
| Thermocouple reference bridge | 1 per experiment | Mounted on the radiation plate of the electronics box | -- | -- | 253 to 363 | ±0.01 |

[a]Gradient-bridge measurements of temperature difference are made at 2 sensitivities, with a ratio of 10 to 1.

by making all bridge measurements with bipolar excitation and by measuring the ratio of the output voltage to the excitation voltage (fig. 11-2).

## EMPLACEMENT OF THE EXPERIMENT AT THE HADLEY RILLE SITE

Drilling of the holes to emplace the heat-flow probes was more difficult than had been expected. The resistant nature of the subsurface at the Hadley Rille site prevented penetration to the planned depth of 3 m. Instead, at the probe 1 site, the borestem penetrated 1.62 m (fig. 11-3); and, at the probe 2 site, the borestem penetrated approximately 1.60 m. The configuration of the probe in each hole is shown in figure 11-3. An obstruction, which was probably a break in the stem at a depth of approximately 1 m, prevented probe 2 from passing to the bottom of the borestem. Because of the very large temperature differences over the upper section, which extends above the surface, no valid temperature measurements were obtained by the ring and gradient bridges on the probe 2 upper section during most of the lunation cycle.

The shallow emplacement of the probes resulted in five of the cable thermocouples lying on, or just above, the lunar surface. These cable thermocouples come into radiative balance with the lunar surface and space, and the measured temperatures can be interpreted in terms of lunar-surface brightness temperatures. A sixth thermocouple is in the borestem projecting above the lunar surface at the probe 1 site.

When this section was written, surface-temperature and subsurface-temperature data had been recorded for nearly one and a half lunation cycles. During the first lunar noon (August 6), a full eclipse of the Sun by the Earth occurred. The thermocouples recorded surface-temperature data at 54-sec intervals during this eclipse. Six in situ conductivity measurements for the low range of values also have been conducted. Only three of these measurements are reported herein.

## SUBSURFACE TEMPERATURES

The surface-temperature measurements during the lunar night and during the August 6 eclipse indicate that the surface layer surrounding the probes has an extremely low thermal conductivity. The subsurface measurements reveal that the conductivity must increase substantially with depth, and values of approximately $1.5 \times 10^{-4}$ W/cm-K are found at a depth of 1 m. With these values of conductivity, it is unlikely that any measurable time variation of temperature as a result of the diurnal cycle existed at depths below 50 cm before the borestem and the heat probe were emplaced. However, after emplacement, the relatively high thermal conductance of the borestem and the radiative transfer along the inside of the stem allowed surface-temperature varitions to penetrate to greater depths. After several lunations, a new periodic steady-state condition will be established

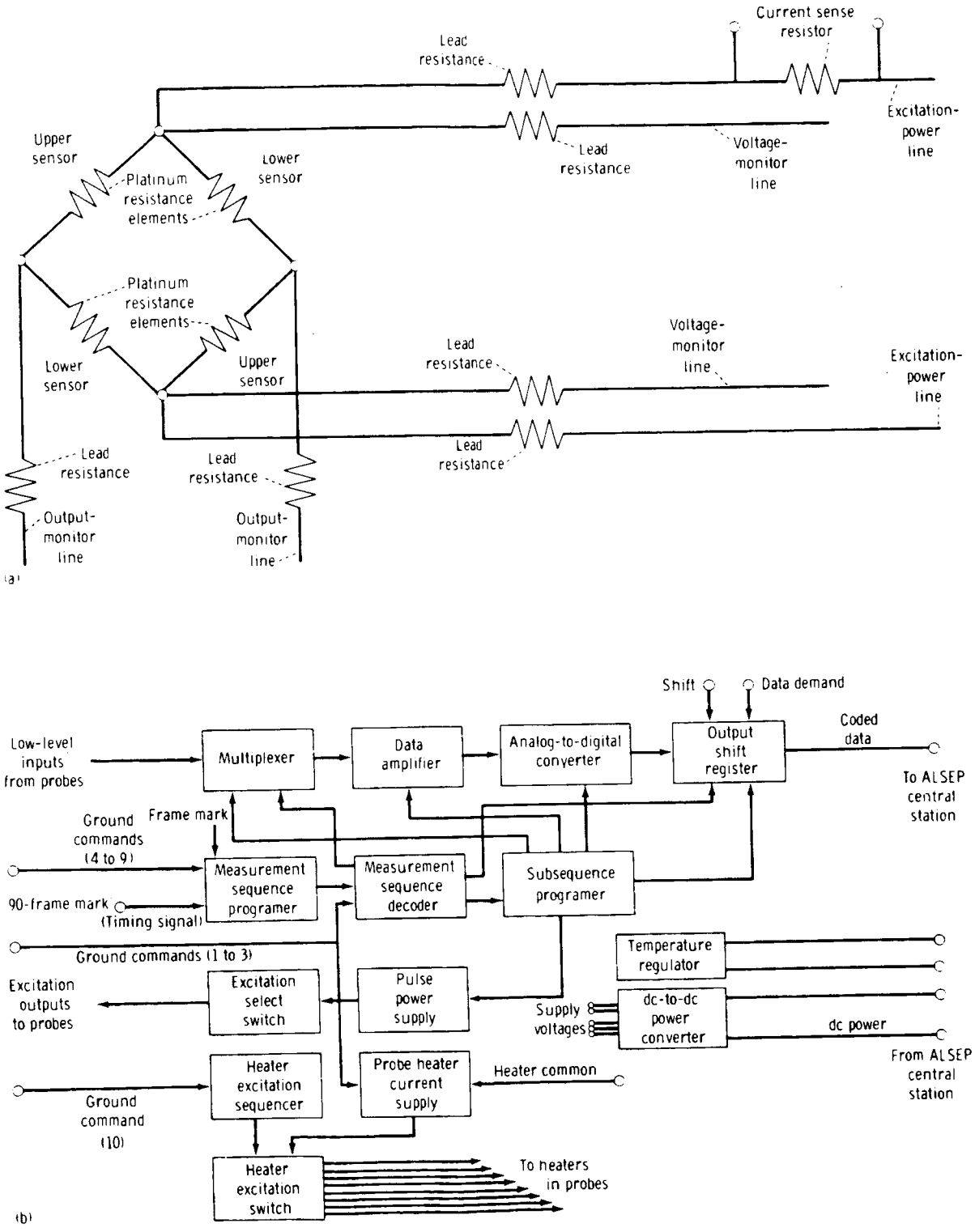


FIGURE 11-2.–Heat-flow experiment. (a) Circuit diagram of the differential thermometer. (b) Block diagram of the experiment electronics.

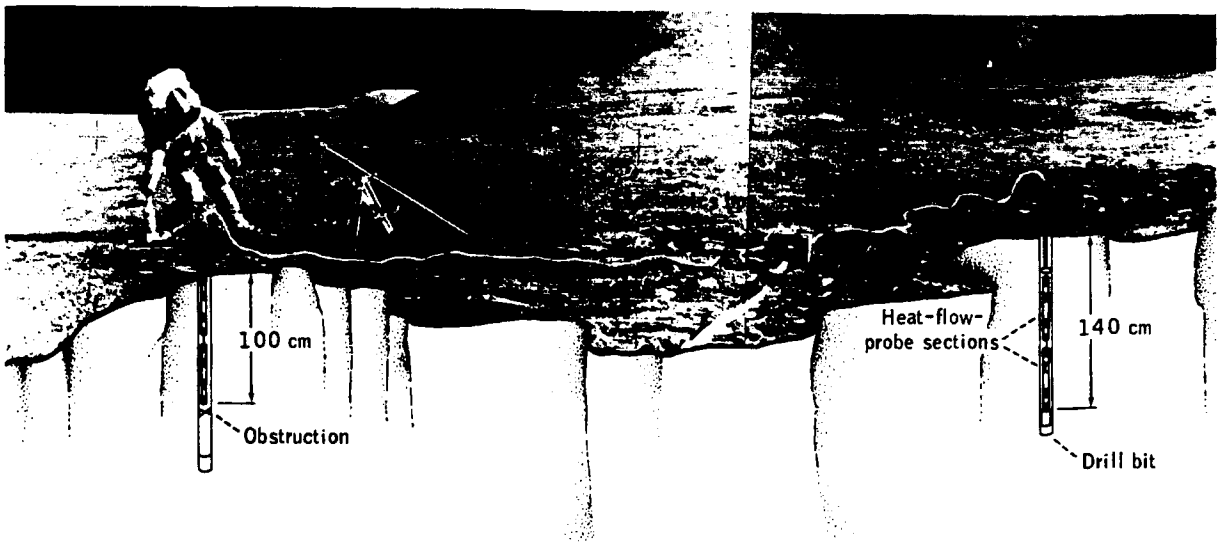


FIGURE 11-3.–Panorama of the heat-flow-experiment emplacement site (composite of photographs AS15-87-11847 and AS15-87-11848) and a cutaway drawing of the heat-probe and thermocouple locations.

around the borestem; initially, however, the borestem and probes will equilibrate toward temperatures that existed in the subsurface before emplacement. By applying the theory of the cooling of a cylinder, which is discussed in the appendix of this section, it is possible to deduce the undisturbed temperature profile at depths where diurnal variations are negligible and to obtain some estimate of the thermal properties of the regolith from the first few hundred hours of equilibration.

The temperature histories of all subsurface thermometers and the evolution of the profiles of temperature as a function of depth for probes 1 and 2 are shown in figures 11-4 and 11-5, respectively. All sensors initially cooled very rapidly, and those sensors at depths greater than 0.7 m continued to cool monotonically with time and were still cooling after 300 hr. The thermometers at depths less than 0.7 m responded to the high temperatures of the borestem projecting above the surface. The temperature in the top of the probe 1 borestem, which is projecting above the surface, was 348 K at lunar noon. As shown in figure 11-5, an obstruction prevented heat-flow probe 2 from passing to the bottom of the hole; consequently, the platinum-resistance thermometers in the top section are not on scale. The cooldown duration of probe 2 is longer than that of probe 1, probably because of the lower conductivity material surrounding the borestem and the higher initial heat input that resulted from extended drilling.

## Extrapolation to Equilibrium Values

To extrapolate the sensor temperatures to equilibrium values, the first-order approximation of the long-term solution of the cooling-cylinder problem

$$\frac{T - T_\infty}{T_0 - T_\infty} = \left(\frac{4\pi kt}{S_1 + S_2}\right)^{-1} \qquad (11\text{-}2)$$

is used, where $T$ is the absolute temperature of the probe in K, $T_\infty$ is the true equilibrium temperature of the probe, and $T_0$ is the probe initial temperature; and where $S_1$ and $S_2$ are the thermal heat capacities per unit length of the inner and outer cylinders, respectively, in W-sec/cm-K, and $t$ is time in seconds. A more complete discussion of the derivation of equation (11-2) and definitions of the variables can be found in the appendix of this section.

If an initial estimate of the equilibrium temperature $T'_\infty$ is made, it can be shown that the error in the estimate $\delta$ is given by

$$\delta = \frac{v_1' - v_2' \frac{t_2}{t_1}}{\frac{t_2}{t_1} - 1} \qquad (11\text{-}3)$$

where $v_1 = T_1 - T_\infty'$, $v_2' = T_2 - T_\infty'$ and $T_1$ and $T_2$ are two temperatures selected from the long-term cooling history at times $t_1$ and $t_2$, respectively. Then the true equilibrium temperature is simply $T_\infty' + \delta$. The equilibrium temperature determined in this way is independent of the initial-temperature estimate. The equilibrium temperatures for all sensors not affected by the diurnal variation are shown in table 11-II. The values also are plotted as functions of depth in figures 11-4 and 11-5. The accuracy of these equilibrium temperatures is ±0.05 K.

At the probe 1 site, the subsurface temperature, which increases regularly with depth, is approximately 252.0 K at a depth of 80 cm. The increase along the lower 60 cm of probe 1 is approximately 1 K. For probe 2, the temperature at a depth of 80 cm is approximately 250.5 K. The two probe 2 sensors that are unaffected by the diurnal variations indicate an increase in temperature with depth at a rate comparable to the rate detected by the probe 1 sensors. This gradient in temperature is a result of the outward flow of heat from the Moon.

## Equilibrium Temperature Differences Along the Heat-Flow Probes

The gradient and ring bridges enable measurement of temperature differences between points 47 cm and 28 cm apart on the probe with an accuracy of ±0.001 K, which is far greater than the accuracy of the absolute-temperature measurements. An analysis similar to that used for the equilibration of the individual sensors can be used to extrapolate the temperature differences to equilibrium values. By using the first term of equation (11-13) in the appendix, the equilibrium temperature difference $\Delta T_\infty$ between two points on the probes is given by the expression

$$\Delta T_\infty = \frac{\Delta T_1 - \Delta T_2 \frac{t_2}{t_1}}{1 - \frac{t_2}{t_1}} \qquad (11\text{-}4)$$

where $\Delta T_1$ and $\Delta T_2$ are temperature differences measured at times $t_1$ and $t_2$, respectively. Equation 11-4 is valid only for very long times ($t > 300$ hr); consequently, only those differential thermometers that have not been affected by the diurnal variations in the first few hundred hours of observation can be used in this analysis.

The only differential thermometers that have not been affected by the diurnal variations are those on the bottom section of probe 1. The calculated equilibrium-temperature difference across the gradient bridge on the bottom section of probe 1 is 0.779 K and, across the ring bridge, 0.483 K. These results can be interpreted in terms of the temperature difference between adjacent points on the borestem wall by taking into account the effect of radiative

TABLE 11-II.–*Lunar Conductivities Determined From Heat-Probe and Cooldown Histories*

| *Sensor* | *Depth, cm* | *Equilibrium temperature, K* | *Minimum-conductivity case* | | *Maximum-conductivity case* | |
|---|---|---|---|---|---|---|
| | | | *Initial temperature, K* | *Deduced conductivity, W/cm-K* | *Initial temperature, K* | *Deduced conductivity, W/cm-K* |
| TG11B | 83 | 251.96 | 315 | $0.8 \times 10^{-4}$ | 349 | $1.5 \times 10^{-4}$ |
| TR22A | 87 | 250.53 | [a]323 | 1.1 | -- | -- |
| TG12A | 91 | 252.28 | 317 | 1.2 | 349 | 1.7 |
| TG22B | 96 | 250.70 | [a]323 | 1.2 | -- | -- |
| TR12A | 100 | 252.40 | 317 | 1.2 | 349 | 1.7 |
| TR12B | 129 | 252.87 | 313 | 1.9 | 349 | 2.9 |
| TG12B | 138 | 253.00 | 313 | 2.1 | 349 | 3.3 |

[a]The borestem at the probe 2 site was drilled down approximately 1 m during the first extravehicular activity (EVA). During EVA-2, 22 hr later, the borestem was drilled an additional 3 min to a depth of approximately 1.5 m. The initial temperature was estimated by calculating the cooldown from the preemplacement temperature for 22 hr between the EVA periods and adding the additional heat of drilling during EVA-2. This procedure resulted in an estimate of initial temperature (323 K) very close to the value determined by extrapolation of temperature data in the 1st hour after insertion.

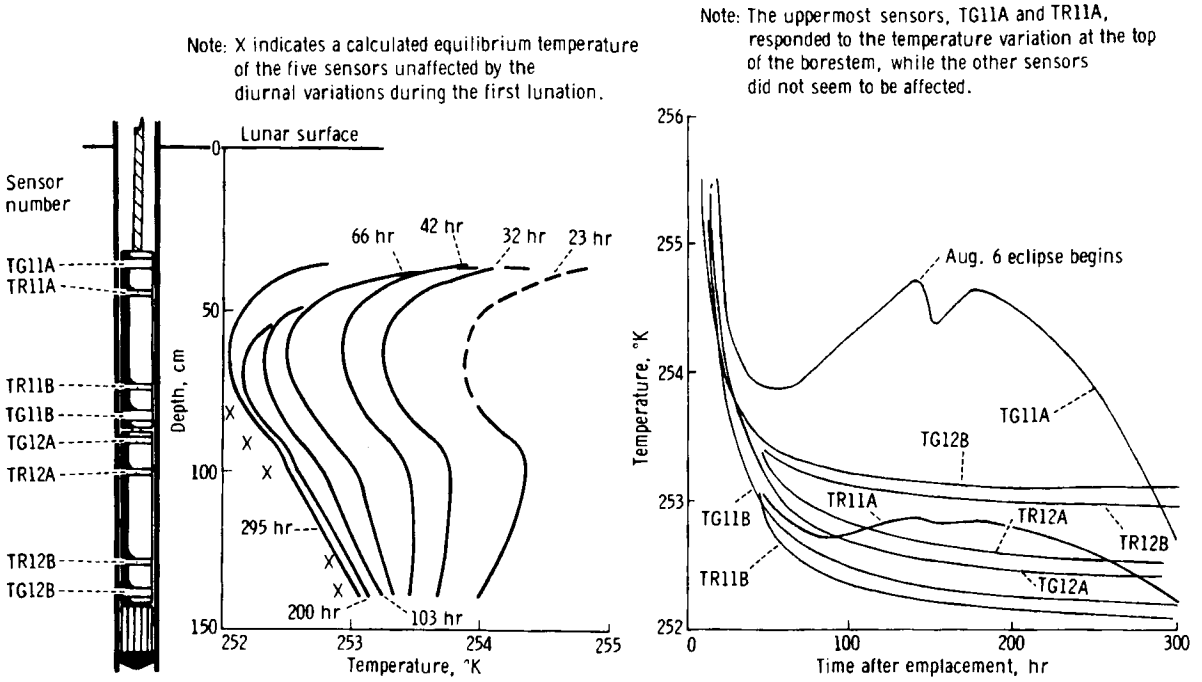


FIGURE 11-4.–Temperature histories of the sensors on heat probe 1 during the first 300 hr after emplacement. The subsurface geometry of the probe and temperature as a function of depth are shown on the left. Temperature as a function of time is shown on the right.

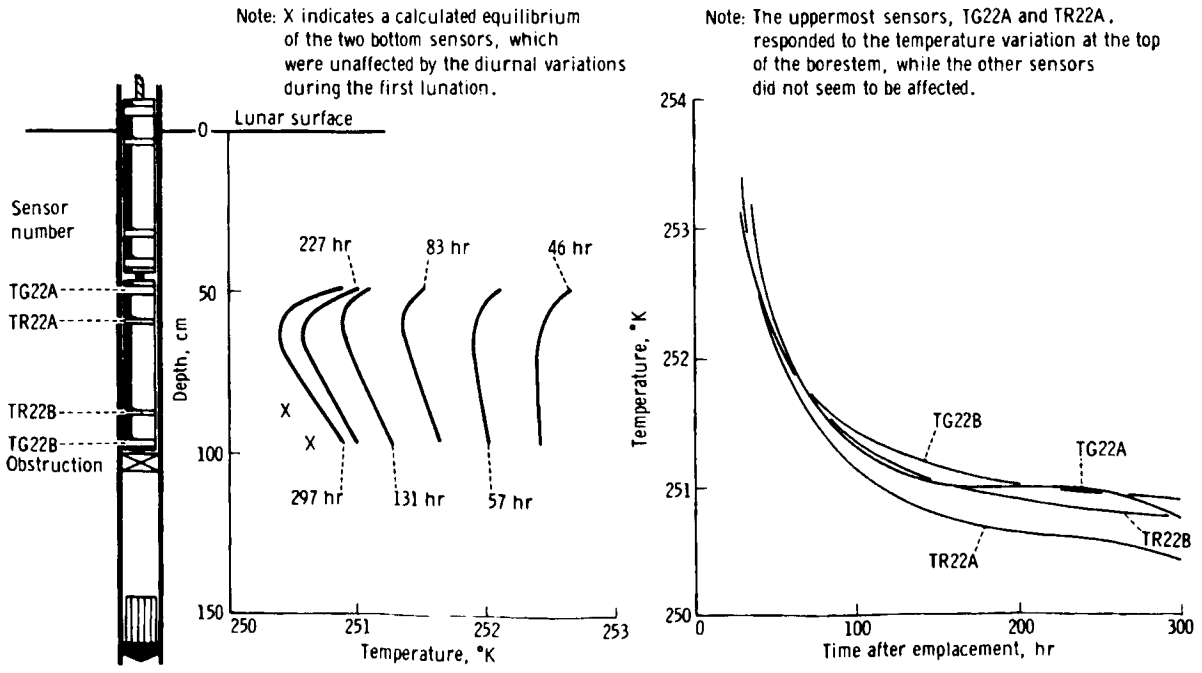


FIGURE 11-5.–Temperature histories of the sensors on heat probe 2 during the first 300 hr after emplacement. The subsurface geometry of the probe and temperature as a function of depth are shown on the left. Temperature as a function of time is shown on the right.

TABLE 11-III. *Summary of Equilibrium-Temperature-Difference Measurements and Subsurface-Temperature Gradients*

| *Differential thermometer* | *Equilibrium temperature difference, K* | | *Lunar temperature gradient, K/m* |
|---|---|---|---|
| | *Probe* | *Borestem* | |
| Gradient bridge | 0.779 | 0.819 | 1.74 |
| Ring bridge | .483 | .502 | 1.77 |

coupling between the walls and the probe and the finite axial conductance of the probe. The temperature difference over the probe is always slightly less than the temperature difference between the adjacent points on the borestem. The ratio of the two, which is called the shorting ratio, was determined experimentally in the laboratory for each section of the probes. The temperature differences at points in the borestem adjacent to the differential thermometers after the shorting ratio has been applied are listed in table 11-III.

The relatively high axial conductance of the borestem results in some axial shunting of the steady-state heat flow; therefore, to determine the undisturbed gradient (i.e., the gradient at large radial distances from the borestem), some correction must be made. The shunting effect can be estimated by modeling the borestem as a prolate spheroid surrounded by a medium with a lower conductivity. By using an effective axial conductivity of $2.3 \times 10^{-3}$ W/cm-K for the borestem and a lunar conductivity of $1.7 \times 10^{-4}$ W/cm-K, the model indicates that a plus-1-percent correction should be applied to the borestem temperature gradients. This correction has been applied to the temperature gradients listed in table 11-III.

## Diurnal Temperature Variations

Variations in temperature synchronous with the solar phase were observed at depths as great as 70 cm during the first one and a half lunations after emplacement. The temperature variations measured by probes 1 and 2 are shown in figures 11-6 and 11-7, respectively. The peak-to-peak amplitude of the variation at the top of probe 1 is approximately 6 K, a 43-to-1 attenuation of the 260 K temperature excursion measured in the part of the borestem that projects above the lunar surface. The ring sensor TR11A, which is located 9 cm below the top of the probe, measured variations with a 2 K amplitude. The sensors on the lower section of probe 2 that detected variations are somewhat deeper (49 and 58 cm) and recorded correspondingly smaller amplitudes. There are two interesting features of the observed variations. The phase shift of the peaks is extremely small, in view of the large attenuation factors, and a considerable portion of the high-frequency component of the solar radiation penetrates to these depths, as indicated by the rapid rates of temperature change at dawn and sunset. These features suggest that much of the heat transfer to the probe occurs by direct radiative exchange with the upper part of the borestem. The thin, aluminized Mylar disk that is located on top of each probe as a radiation shield apparently does not prevent significant radiative exchange between the top of the probe and the lunar surface.

The heat exchange during a lunation cycle is very complex, because the borestem conducts heat from and toward the lunar surface more efficiently than the regolith material. Thus, the low nighttime temperatures penetrate downward along the borestem, which enlarges the low-temperature area viewed by the top of the probe and, hence, increases the heat loss from the probe to the surface. A similar, but opposite, effect occurs during the day. This phenomenon may, in part, explain the asymmetry of the plots of temperature as a function of time.

Diurnal temperature variations that propagate along the borestem have an important effect on the mean temperature in the borestem. Because the conductivity of the borestem is not as temperature dependent as the adjacent lunar material, heat will be lost more readily along the borestem at night. Consequently, the heat balance over a full lunation will require that the borestem, to depths that diurnal variations penetrate, have a lower mean temperature at a given depth than the regolith. Thus, a net cooling of the borestem in the upper meter can be anticipated, which is an effect that is already apparent in the substantial decrease in peak temperature during the second lunation. Comparisons with the cooling curves of deeper sensors show that this difference cannot be explained by cooling from initial temperatures alone. This cooling effect results in a gradient in mean temperature in the upper meter of the borestem that is unrelated to the heat flow from the interior.

It is essential to note that the mean temperatures and temperature differences in those sections of the

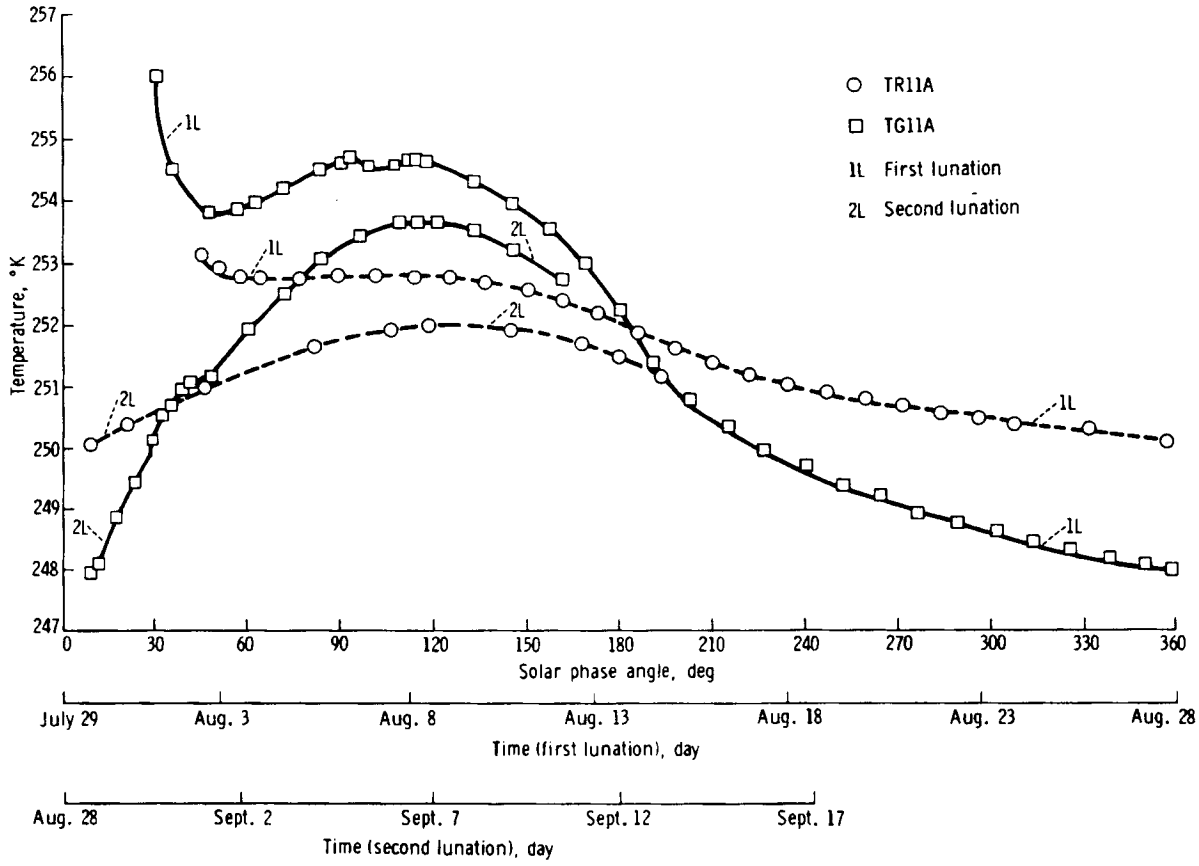


FIGURE 11-6.–Temperature as a function of solar phase angle for probe 1 sensors TR11A and TG11A (the sensors that detect diurnal variations) for the first one and a half lunations after emplacement.

borestem that see diurnal variations cannot be used to determine gradients related to the heat flow from the lunar interior until the effect of temperature-dependent conduction in the borestem and the surrounding lunar material is analyzed and the effect quantitatively determined. Such an analysis is beyond the scope of this preliminary report, but the analysis will be made on future subsurface-temperature data after the upper part of the borestem has equilibrated nearer to the mean periodic steady-state temperature. This analysis will add two independent measurements of heat flow to the result already reported here.

## Implications of the Large Mean-Temperature Gradients in the Upper 50 cm at the Hadley Rille Site

By using a finite-difference model to generate daytime lunar-surface temperatures (which depend almost exclusively on the solar flux) and by using the reduced thermocouple temperatures to obtain lunation nighttime surface temperatures, a mean lunar-surface temperature of 217 K (±3 K) was obtained. This result indicates an increase in mean temperature (35 K higher than the mean surface temperature) at depths beyond which the diurnal variation penetrates. This phenomenon can be explained in terms of a strong temperature dependence of the thermal conductivity, which previously has been investigated by Linsky (ref. 11-4) and others. Because of the near lack of an atmosphere on the Moon, radiative transfer of heat between and through particles of the lunar fines can contribute significantly to the effective thermal conductivity. This temperature-dependent conductivity has been found to obey a relation of the form (ref. 11-3)

$$k(T) = k_c + k_r T^3 \qquad (11\text{-}5)$$

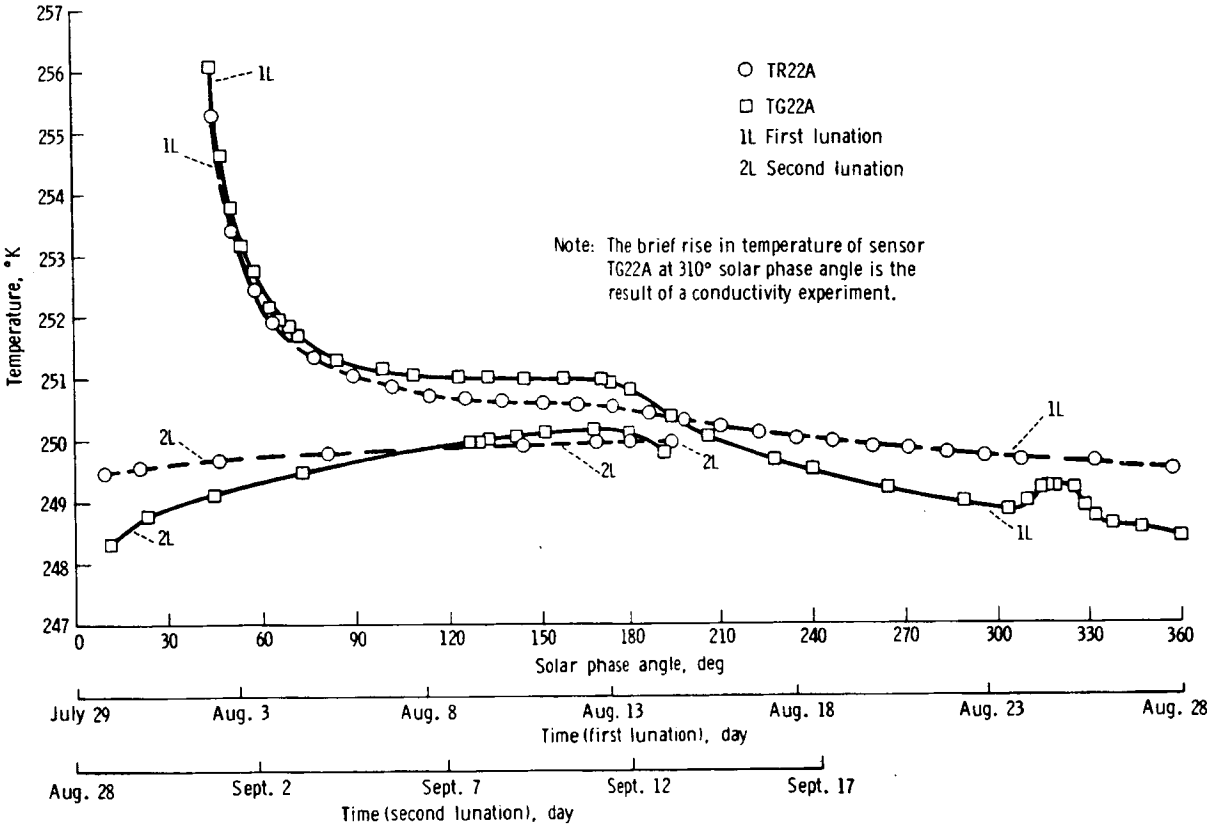


FIGURE 11-7.–Temperature as a function of solar phase angle for probe 2 sensors TR22A and TG22A (the sensors that detect diurnal variations) for the first one and a half lunations after emplacement.

where $k_c$ is the contribution from conduction and $k_r T^3$ represents the radiative exchange between and through particles. Linsky (ref. 11-4) has used computer models of the lunar surface to evaluate this effect in the absence of a steady-state heat flow. By interpolating from these models, the relative contributions of the conductive and radiative terms can be estimated. For a difference of 35 K in mean temperature between the surface and depths at which no significant time variations of temperature exist, the ratio of radiative to conductive terms is approximately 2 at a temperature of 350 K. The relatively small steady-state gradient (1.75 K/m) produced by the measured steady-state heat flow will have only a slight effect on this ratio. Conductivity measurements have been performed for a wide range of temperatures on returned lunar samples from the Apollo 11 and 12 missions (ref. 11-9). The results also indicate the significant temperature dependence of conductivity. For Apollo 11 and 12 samples, the data cited in reference 11-9 indicated that the ratios are 0.5 and 1.5, respectively. The conductivity of the more highly temperature-dependent lunar fines from the Apollo 12 site seem to be more comparable to the upper regolith conductivity at the Hadley Rille site. Further refinement of surface-thermocouple data, combined with a more accurate determination of conductivity as a function of depth and direct measurements of the conductivity of returned Apollo 15 samples, will result in the first directly measured profile of regolith conductivity to a depth of 1.5 m.

## CONDUCTIVITY OF THE REGOLITH

### Preliminary Deductions from the Heat-Flow-Probe Histories

The rate of equilibration of the probes depends on the thermal diffusivity $\kappa$ of the surrounding lunar material, the ratio $\alpha$ of heat capacity per unit volume

of the lunar material to the heat capacity per unit volume of the heat probe, and the contact conductances $H_1$ and $H_2$, where

$$\alpha = 2\pi b^2 \rho c/(S_1 + S_2)$$

$c$ = heat capacity per unit mass of the surrounding lunar material, W-sec/cm-K

$\rho$ = density of the surrounding lunar material g/cm$^3$

$H_1, H_2$ = contact conductances of the inner- and outer-cylinder boundaries, respectively, W/cm$^2$-K

A more complete discussion can be found in the appendix of this section. By using an estimate of the volumetric heat capacity of the lunar material $\rho c$, a value for $\alpha$ can be determined, because the thermal properties of the probe and the borestem are known. From an analysis of the cooling history of the probes, an estimate of the diffusivity, and, thus, the conductivity, can be made. Measurements of the heat capacity of samples that represent a wide range of lunar rock types result in very uniform values (ref. 11-10). The density of the regolith material is quite variable; preliminary measurements of samples taken by core tubes at the Hadley Rille site result in values that range from 1.35 to 1.91 g/cm$^3$. At the depth of the probes, the densities are probably near the high end of this range and not so variable. For the analysis described in this section, a density of 1.8 g/cm$^3$ and a heat capacity of 0.66 W-sec/g-K have been assumed.

It is not possible to determine a value of $\kappa$ from the ratios of temperatures at various times during the cooldown, because, as the long-term solution indicates, the temperature ratios depend solely on the ratio of the times. Bullard (ref. 11-11) has pointed out this property of cooling cylinders in his discussion of sea-floor heat-flow measurements. To estimate a value for $\kappa$, the initial temperature must be known. Estimates of the initial temperature can be made by extrapolating data recorded soon after the probes were inserted to the time the borestem was emplaced. This estimate is considered to be a minimum value, because cooling during the first several minutes is faster as a result of enhanced radiative transfer at high temperatures. Alternately, the assumption can be made that the initial temperature is the temperature of the borestem before emplacement, plus some estimated temperature rise as a result of the heat produced during drilling. Temperatures recorded before emplacement by probe 2, which was stored temporarily in the drill rack between EVA-1 and EVA-2, were used as estimates of the borestem temperature before emplacement. The temperature rise that resulted from drilling is estimated to be 15 K/min, based on estimated torque levels. The initial-temperature estimates based on these assumptions are considered to be maximum estimates.

The cooling histories of all subsurface sensors that are not affected by diurnal variations were analyzed to determine the conductivity of the surrounding lunar material for the two limiting estimates of initial temperature. By using the equilibrium temperature $T_\infty$ for each sensor, the ratio $(T-T_\infty)/(T_0-T_\infty)$ was determined for the first few hundred hours of equilibration. A typical plot of this ratio as a function of time is shown in figure 11-8. The procedure for determining conductivity is to make an initial estimate of the parameters $h$ and $A$, where

$$h = k/bH_2$$

$$A = S_2\gamma\kappa/b^2(S_1 + S_2)$$

$$\gamma = S_1/2\pi aH_1$$

$a$ = radius of the inner cylinder (heat-flow probe) in centimeters

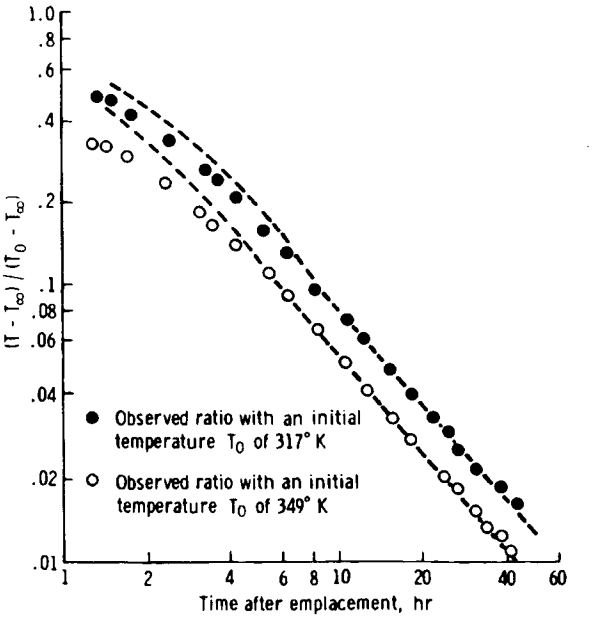


FIGURE 11-8.–Ratio of temperatures measured by sensor TG12A during the initial equilibration of heat probe 1 with the lunar subsurface compared with the theoretical cooldown curves computed from equation (11-12) (dashed lines).

Then, by equating observed temperature ratios for several times in the cooling history with the ratios computed from equation (11-12) in the appendix, a value for the dimensionless parameter $\tau$ can be found that corresponds to each time. Once a value for $\tau$ is known, $k$ can be determined from the relation $\tau = kt/\rho cb^2$. The conductivity value determined for a large value of $\tau$ will be the most accurate, because, at long times, $f(A,h,\alpha,\tau)$ is nearly independent of $h$ and $A$, where $f(A,h,\alpha,\tau)$ designates the right-hand side of equation (11-12) in the appendix. By using this initial long-time estimate and comparisons of observed and computed ratios at early times, a best value of $k$ and $H_2$ can be determined with two or three repetitions of the procedure.

Theoretical curves fitted to the data obtained from sensor TG12A by this procedure and ratios for both limiting initial-temperature estimates are shown in figure 11-8. The parameters $h$ and $A$ have been chosen to fit data for times greater than 6 to 8 hr. The theoretical curve at earlier times lies well above the observed data; however, it is not possible to find a value for $H_2$ to fit data obtained at times earlier than 6 hr without degrading the fit at later times. To obtain the most accurate value of $k$, the curve must be fit to the data for large values of $\tau$.

In table 11-II, the maximum and minimum conductivity values determined by the procedure are shown arranged in order of increasing depth. The conductivities that were determined for minimum and maximum initial-temperature estimates differ, on the average, by 50 percent. The more accurate conductivity measurements, which were made by using the heaters that surround the gradient sensors, resulted in values that lie within the ranges listed in table 11-III. The deduced conductivity values are considerably higher than the value obtained from measurements on returned lunar fines. The value for the returned lunar fines is approximately $2.2 \times 10^{-5}$ W/cm-K at 250 K (ref. 11-12). The higher conductivity values that were obtained may be representative of fragmental regolith material in a more dense and compressed state than the surface fines.

## In Situ Measurements

Six in situ conductivity measurements in mode 2, which is the low-conductivity mode, were conducted at the end of the first lunar night and during the first half of the second lunar day. The two heaters on the upper section of probe 2 were not turned on because the gradient bridges were off scale. The mode 2 measurements indicated the subsurface conductivity to be in the lower range of measurement and, in addition, showed that a substantial contact resistance exists between the borestem and the lunar material. A decision was made, therefore, not to run the mode 3 (high-conductivity mode) measurements at this time because of the possibility that the gradient sensors might reach temperatures potentially dangerous to the sensor calibration. Mode 3 measurements are planned at some future time after the effects of heater turnon are examined by using the conductivities determined from the mode 2 results.

Three of the conductivity measurements have been analyzed. Two of these measurements were obtained by the use of heaters on the lower section of probe 1, the section across which the best temperature gradient was determined. The third measurement was obtained by the use of the upper heater on the lower section of probe 2.

The interpretation of the response of the temperature-gradient sensor to heater turnon, in terms of the lunar conductivity, is accomplished by using a detailed finite-difference model (ref. 11-13). A simple analytical model of the gradient-sensor long-term ($t >$ 20 hr) performance deduced from the experimental data and the finite-difference models will be briefly discussed in the following paragraphs.

The temperature increase as a function of time at a given heater-sensor location upon heater turnon depends on the quantity of heat generated and the rate at which the generated heat can diffuse outward from the heater source. This rate will depend on the thermal properties of the material that surrounds the source. The heat will propagate axially along the probe and radially from the probe to the drill casing, across the contact-resistance layer outside the casing, and into the lunar medium. Both radiative transfer and conductive transfer are involved in the dissipation of heat. Shortly after heater turnon, the rate of temperature increase at the gradient sensor will depend primarily on the thermal properties of the probe and the borestem in the immediate vicinity of the heater and on the resistive gaps between the probe and the borestem and between the borestem and the lunar material. As the near-sensor probe parts and the borestem temperature increases, a temperature drop is established across the resistive gaps. When this temperature difference builds to a relatively large

value, heat will flow out from the borestem, across the contact-resistance gap, and into the medium; and the rate of temperature increase at the sensor will level off. At long times (times greater than 1000 min in this experiment), the temperature increase $\Delta v(t)$, measured at the sensor, closely fits a relation of the form

$$\Delta v(t) = C_1 \ln(t) + C_2 \qquad (11\text{-}6)$$

where $C_1$ and $C_2$ are constants that depend on the contact conductances $H_1$ and $H_2$ and the properties of the lunar material. The finite-difference thermal model of the probe in the lunar material shows the same long-term characteristics. This relationship has the same form as the long-term solution to the problem of a uniformly heated infinite cylinder (ref. 11-14). As in the case of the long-term solution for a cylinder, it has been determined from the finite-difference models that, at long times after heater turnon, the constant $C_1$ is almost solely a function of the conductivity of the surrounding material and the heat input. Thus, the slope $[\Delta v(t_2) - \Delta(t_1)]/\ln(t_2/t_1)$, for times greater than 1000 min, is a sensitive measure of the conductivity of the surrounding material for a constant heat input. Plots of temperature increase as a function of time for the three conductivity measurements are shown in figure 11-9 and compared with best-fitted theoretical models.

The magnitude of temperature increase at any time greater than 0.5 hr after heater turnon is very sensitive to the magnitude of the contact conductance $H_2$. The value of the contact conductance, however, has no detectable effect on the slope of the curve of $\Delta v$ as a function of $\ln(t)$ at long times; therefore, the determination of a value for $k$ can be made independently of $H_2$ by matching slopes at times greater than 1000 min. By using this value of $k$, a value for $H_2$ was determined by varying $H_2$ in the finite-difference models until the experimental curves of $\Delta v$ as a function of $t$ were bracketed within a small tolerance. Examples of models that bracket the experimental curves of the three in situ experiments are shown in figure 11-9.

A rather accurate determination of the conductivity of the lunar subsurface material that surrounds each heater location can be made. For example, at heater location H23 (the location of sensor TG22A), the long-time slope data could be bracketed by models of $k = 1.3 \times 10^{-4}$ and $k = 1.4 \times 10^{-4}$ W/cm-K. A linear interpolation between these models resulted in a value $k = 1.37(\pm 0.02) \times 10^{-4}$ W/cm-K. However, the assumption cannot be made that the models represent the physical situation this accurately; a value $k = 1.4(\pm 0.1) \times 10^{-4}$ W/cm-K would be more realistic. Further examination of the effects of the errors introduced by the assumptions about the model parameters (probe properties, heat-transfer linkages, etc.) must be made so the actual precision of the $k$ values can be determined. From previous limited parametric studies, a range of ±10 percent should represent a maximum bound in the error of the $k$-value determinations.

The best determinations of conductivity values are listed in table 11-IV. As shown in the table, the conductivity determinations from the heater experiments fall within the range of the $k$ predictions of the initial probe cooldown analyses and indicate a significant increase of conductivity with depth.

The contact-conductance values determined from the in situ measurements vary. The contact conductance probably corresponds to a thin zone around the borestem that is filled with lunar fines. If the assumption is made that these fines have a conductivity of $2 \times 10^{-5}$ W/cm-K, which is similar to the conductivity of the surface fines, the widths of the disturbed zones would be 2.7, 2.0, and 1.3 mm for the locations of sensors TG22A, TG12A, and TG12B, respectively. The larger value of $H_2$ at the location of sensor TG12B might result from greater compaction of the fines, rather than a thinner zone. The thicker disrupted zone around probe 2 may have resulted from the longer period of drilling.

## STEADY-STATE HEAT FLOW FROM THE LUNAR INTERIOR BELOW THE HADLEY RILLE SITE

The conductivity of the regolith is shown by the measurements returned from the experiment to be significantly variable with depth over the lower section of probe 1. To compute the heat flow from temperature differences over a finite depth interval, the thermal resistance must be known. The thermal resistance can be calculated from the equation

$$R_{x_1 - x_2} = \int_{x_1}^{x_2} \frac{dx}{k(x)} \qquad (11\text{-}7)$$

where $x_1$ and $x_2$ are the end points of the interval.

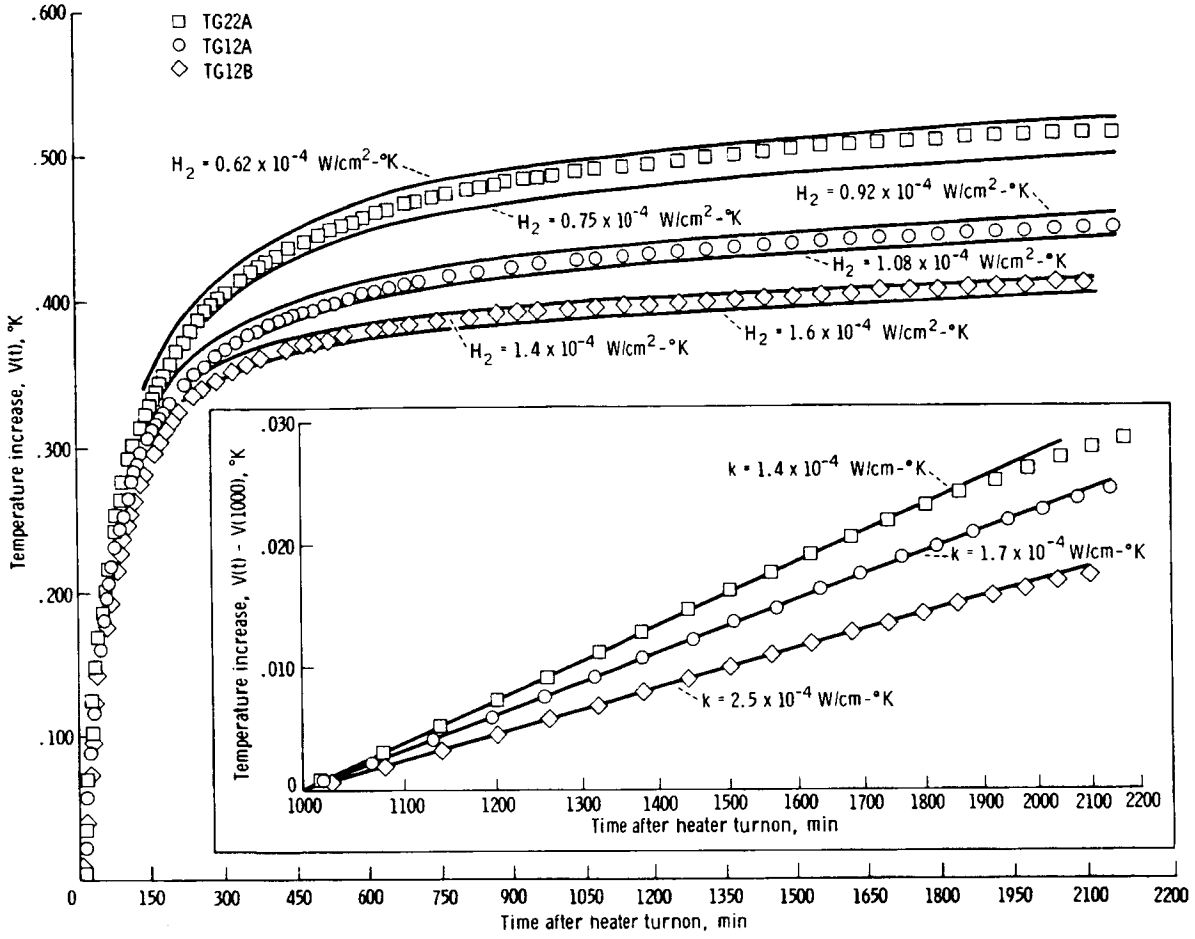


FIGURE 11-9.–Temperature increase as a function of time after heater turnon for heaters located at sensors TG22A, TG12A, and TG12B. Two computed models that closely bracket the data are shown for each of the three heater locations. Temperature increase as a function of time after 1000 min is shown in the inset on an expanded scale. The solid lines in the inset are best fitting computer models.

TABLE 11-IV.–*Conductivity Determinations From in Situ Experiments*

| *Heater sensor* | *Depth, cm* | *Thermal conductivity,* k, *W/cm-K* | *Contact conductance of the borestem,* $H_2$, *W/cm$^2$-K* |
|---|---|---|---|
| TG22A | 49 | 1.40 (±0.14) x $10^{-4}$ | 0.7 x $10^{-4}$ |
| TG12A | 91 | 1.70 (±0.17) | 1.0 |
| TG12B | 138 | 2.50 (±0.25) | 1.5 |

Thus, for the flux to be determined, $k$-value variation in the interval between the gradient sensors, which are located at depths of 91 and 138 cm, must be known. Accurate measurements of $k$ were made only at the end points; however, a constraint can be applied on the variation with depth from the ratio of the temperature differences measured by the ring bridge and the gradient bridge. If the heat flow is uniform with depth, the constraint required by the ratio of temperature differences is

$$\frac{\int_{100}^{129} \frac{dx}{k(x)}}{\int_{91}^{138} \frac{dx}{k(x)}} = \frac{\Delta T_{ring}}{\Delta T_{gradient}} = 0.613 \quad (11\text{-}8)$$

Three possible conductivity profiles are shown in

figure 11-10. Profile B is based on the trend of conductivities from the cooldown curves and obeys the constraint of equation (11-8). Profile A also obeys the constraint of equation (11-8) but includes a uniform conductivity of 1.7 W/cm-K to a depth of 136 cm and, then, a thin layer with a conductivity of $2.5 \times 10^{-4}$ W/cm-K in which the bottom sensor is embedded. Profile A would result in a lower limit for the heat flow; profile C indicates a uniform increase in conductivity over the probe section. Profile C does not obey the constraint of equation (11-8), but defines an upper limit for the heat-flow value. The trend of conductivity up to a depth of 50 cm that is indicated by the probe 2 measurement makes cases with higher conductivity than shown in profile C unreasonable. Based on these three profiles shown in figure 11-10, the temperature difference over the lower section of probe 1 results in the heat-flow values listed in table 11-V. The uncertainty of the conductivity measurements (±10 percent) should be considered as error bounds on each of the heat-flow values listed in table 11-V.

Analysis of data obtained during a full year will enable the previous determinations to be refined considerably. In addition, a comparison of the value obtained from the bottom section of probe 1 with the values obtained from the upper section of probe 1 and the lower section of probe 2 can be made once an analysis of the effects of the diurnal variations has been completed.

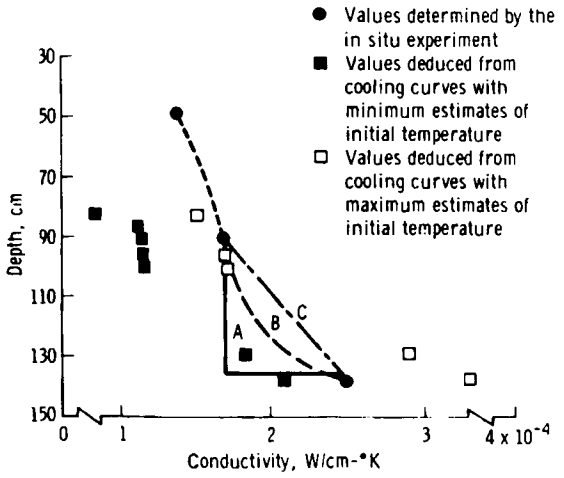


FIGURE 11-10.–Conductivity as a function of depth, with three possible conductivity profiles (A, B, and C) (table 11-V).

TABLE 11-V.–*Heat-Flow Data Obtained From the Lower Section of Probe 1*

| *Profile* | *Heat flow, W/cm²* | *Comment* |
|---|---|---|
| A | $2.99 \times 10^{-6}$ | Lower limit |
| B | 3.31 | Best value |
| C | 3.59 | Upper limit |

## SURFACE TEMPERATURES DEDUCED FROM THE CABLE THERMOCOUPLES

Of the eight thermocouples designed to measure the temperature profile in the upper 1.5 m of the heat-flow borehole, six presently measure temperatures that may be used to deduce the variation of lunar-surface brightness temperature throughout the lunation period. Of particular interest is the determination of temperature during total eclipses and lunar nights, which are measurements difficult to obtain by Earth-based telescopic observation. The thermocouples in the cable of the heat-flow experiment, lying on or just above the lunar surface, provide a means by which these measurements can be obtained at a sampling rate previously unattainable (one measurement set each 54 sec).

During the lunar night, the thermocouples come into radiative balance with the lunar surface and space. To determine the relationship between the cable temperature and the lunar-surface brightness temperature, the heat balance for a small cylindrical cable element of radius $a$ and length $dl$ can be considered. The heat balance for such an element arbitrarily oriented above the lunar surface during the lunar night can be represented by

$$F_{C\text{-}M}\, 2\pi a dl\, \epsilon_{CIR}\, \epsilon_M \sigma T_M^4 - 2\pi a dl\, \epsilon_C \sigma T_C^4 - V\rho c \frac{\partial T_C}{\partial t} = 0 \qquad (11\text{-}9)$$

where the first term is the energy received by the cable element from the Moon per unit time, the second term is the energy lost from the cable element per unit time, and the third term is the energy required to change the temperature of the cable element per unit time; and where

$F_{C\text{-}M}$ = view factor of the cable element to the lunar surface

$\sigma$ = Stefan-Boltzmann constant ($5.67 \times 10^{-8}$ W-sec/m²-K)

$\epsilon_M$ = lunar-surface emittance

$\epsilon_C$ = cable-element emittance
$\alpha_{CIR}$ = cable-element infrared absorptance
$V$ = cable-element volume
$\rho c$ = volumetric heat capacity of the cable element
$T_M$ = lunar-surface brightness temperature
$T_C$ = cable-element temperature

For $\epsilon_M = 1$ and a flat lunar surface, equation (11-9) reduces to

$$T_M^4 = \frac{1}{\alpha_{CIR}} \left( \frac{a\rho c}{\sigma} \frac{\partial T_C}{\partial t} + 2\epsilon_C T_C^4 \right) \quad (11\text{-}10)$$

The term $\frac{a\rho c}{\sigma} \frac{\partial T_C}{\partial t}$, which accounts for the thermal time constant of the cylinder, is retained only for eclipse calculations, because the constant is on the order of minutes.

The orientations of the thermocouples that are outside the borestems are unknown. The time at which a given thermocouple reaches the maximum temperature and the value of that maximum are strong functions of the orientation of the cable section in which the thermocouple is embedded. This effect, which is shown in figure 11-11, is a result primarily of the variation in the incidence angle of the solar radiation; therefore, lunar-surface brightness temperatures deduced during the lunar day are subject to error that results from the orientation uncertainties.

For the calculation of the lunar-surface brightness temperatures, the assumption was made that the view factors from the cable to space and from the cable to the surface are identical. The irregular horizon formed by the Apennine Mountains increases the effective view factor to the lunar surface, and the view factor to space is reduced correspondingly. Some of the thermocouples may be close enough to the surface so that local topographic irregularities affect the horizon seen by the cable. For a 10-percent increase in the effective view area to the topographic surfaces, the calculated surface brightness temperatures would be reduced by 2.25 percent during the lunar night.

A more serious error in lunar-night calculations results from the uncertainty in the values of the cable absorptance and emittance. For the temperatures given in figure 11-12, the emittance-to-absorptance ratio was assumed to be unity. A 20-percent increase in this ratio would result in an increase of 4.5 percent in the calculated value of the surface brightness temperature. A value of 0.97 was chosen for both the cable infrared emittance and absorptance, where the assumption was made that the sections of cable in which the thermocouples are embedded are covered by a significant amount of lunar-surface material. Photographs show that most of the cable areas are coated with lunar material.

The surface-brightness-temperature history for the first lunar night, as deduced from thermocouple temperatures, is shown in figure 11-12. A very rapid cooling of the surface is indicated for the first 80 hr after sunset; subsequently, the rate of cooling slows significantly. A cooling curve (ref. 11-15) based on astronomical observations at two different latitudes is shown for comparison. Two theoretical curves based on finite-difference calculations of thermal models of the lunar surface and subsurface are also shown. Curve A, which is derived from a model with a linear conductivity increase starting at a depth of 8 cm (inset, fig. 11-12), duplicates the rate of cooling for times greater than 80 hr, whereas curve B, which is based on a temperature-dependent-conductivity model (ref. 11-12), duplicates the earlier part of the observed curve. For both models, the heat capacity was defined by the following equation (from ref. 11-16)

$$c(T) = -0.034T^{1/2} + 0.008T - 0.0002T^{3/2} \quad (11\text{-}11)$$

The assumed densities are 1.2 g/cm$^3$ for curve A and 1.0 g/cm$^3$ for curve B. The flattening of the observed curve could, in part, be a result of a significant increase in density in the upper several centimeters.

The temperature dependence of conductivity that is indicated by the cooling curves is in agreement with the large increase in mean temperature described previously. The substantial increase in conductivity and density with depth that is suggested by the flattening of the cooling curves is in agreement with earlier conclusions that were based on astronomical observations (e.g., ref. 11-16). The mechanical properties of the soil measured near the Apollo 15 ALSEP site revealed that the shear strength increased rapidly with depth in the upper 20 cm (sec. 7). This increase in shear strength probably is related to a near-surface density gradient.

Surface brightness temperatures during the umbral stage of the August 6 eclipse were deduced from the

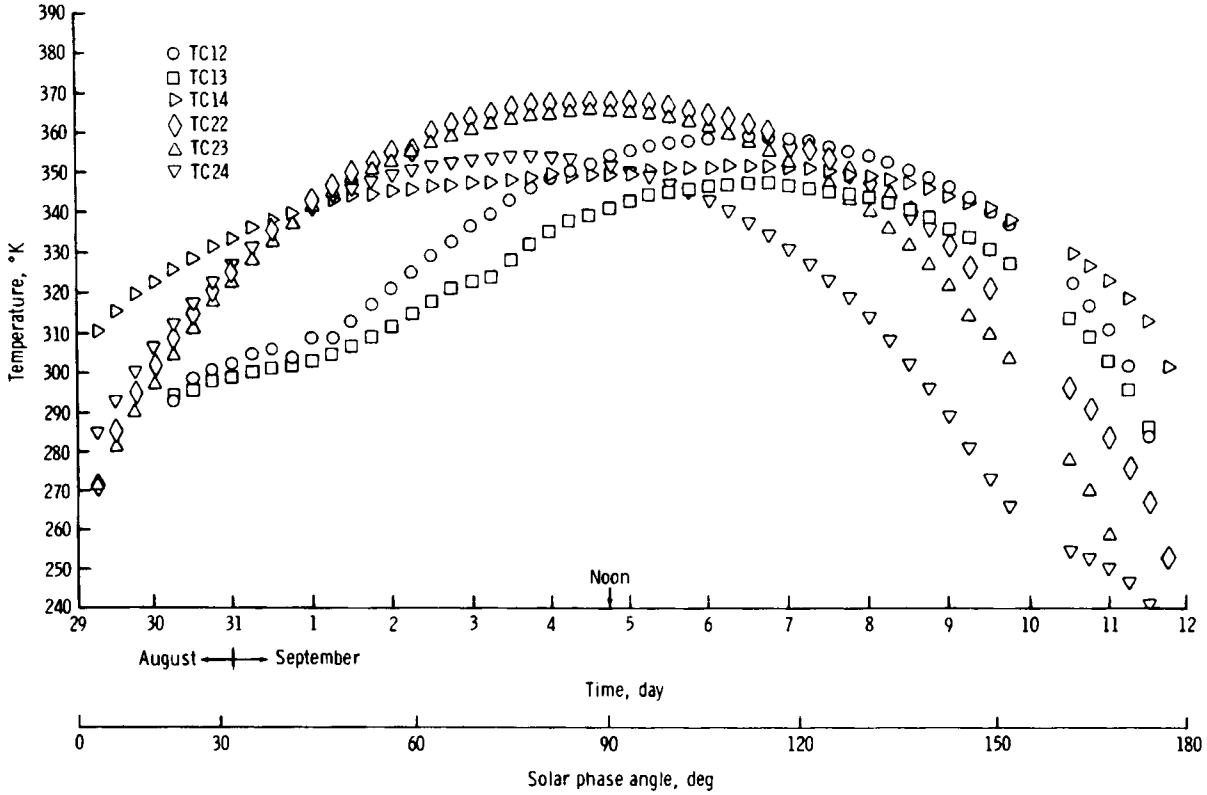


FIGURE 11-11.–Thermocouple temperatures as functions of time for the second lunar day. Thermocouples TC12 and TC13 measure the probe 1 cable temperatures; TC22, TC23, and TC24 measure the probe 2 cable temperatures; and TC14 measures the probe 1 borestem temperature.

thermocouple temperatures. For these calculations, the thermal time constant of the cable must be considered. The thermal mass of the cable per unit length in which the thermocouple is embedded was estimated by summing the properties of the 35 conductors. Uncertainties result from the fact that noise in the thermocouple measurements makes an accurate determination of the slope difficult. A sample of thermocouple data for the later part of the umbra was reduced by determining the rate of change of the cooling curve by graphical techniques. These very preliminary results indicate that the umbral temperatures reached at the lunar surface correspond well with the temperatures predicted by the theoretical curve based on the relationship between conductivity and temperature for lunar fines (ref. 11-12).

In summary, the surface-temperature data for lunar night and the umbral part of the August 6 eclipse support the conclusion that the upper few centimeters of the lunar-surface material have a thermal conductivity-versus-temperature relationship similar to that found for samples of lunar fines measured in the laboratory. The lunar nighttime observations reveal a substantial conductivity gradient with depth that probably results from increasing material density with depth.

## DISCUSSION OF HEAT-FLOW-EXPERIMENT RESULTS

### Local Topographic Effects

The heat-flow determinations at the Hadley Rille site are susceptible to a number of disturbances. Corrections for some of these disturbances (such as the thermal perturbations caused by visible topographic features) can readily be made with sufficient accuracy, but other disturbances may result from refraction associated with sloping interfaces between

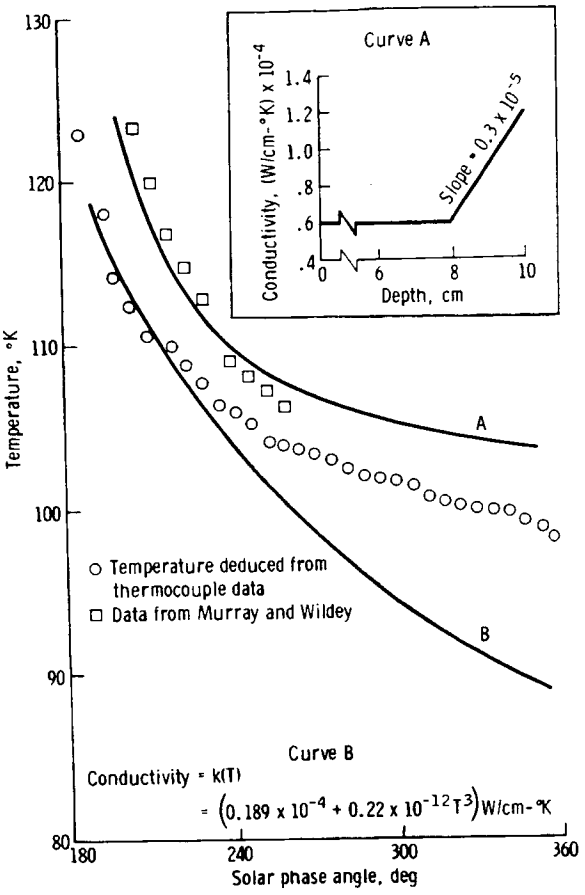


FIGURE 11-12.–Surface cooling as a function of time for the first lunar night, as deduced from thermocouple measurements. Two theoretical curves are given as references. Curve A is the expected curve for a conductivity increase with depth, starting at a depth of 8 cm; curve B is the theoretical curve for a temperature-dependent conductivity. The data from reference 11-16 are included for comparison. Conductivity as a function of depth for the curve A data is shown in the inset.

materials of differing thermal conductivity. Such interfaces, if present at all, are hidden in the lunar interior, and only a qualitative discussion of the effects can be given.

Probe 1, from which data were used for the preliminary determination of heat flow, is located in a small crater that has been almost filled and nearly obliterated by later bombardment. The topography associated with this old crater is so subdued that no correction for the topography is required. However, the possibility remains that the event that produced this crater also locally altered both the thickness and the physical properties of the regolith. The truth of this hypothesis cannot be verified because no observational evidence is available; however, after the data from probe 2 have been analyzed, a comparison of the two heat-flow values may provide more information.

The two most conspicuous and important topographic features near the heat-flow-experiment site are Hadley Rille and the Apennine Front. The topographic effect of the rille was calculated by fitting the rille profile with a two-dimensional Lees-type valley (refs. 11-17 and 11-18). This procedure results in a correction of 4.5 percent, and further allowance for the Elbow, where the rille abruptly changes direction, reduces the correction to 3.5 percent.

A second effect of the topography around the Hadley Rille site is that the surface in the area is shaded during part of the day; consequently, the average surface temperature is lower than flat portions of the lunar surface. This local cold-spot effect has been estimated quantitatively in two ways. The radiation balance for a point halfway down the rille wall (including factors for incoming solar radiation and radiation from the opposite wall), at appropriate times of the lunar day, was calculated and used to derive the mean temperature in the rille. Alternatively, the temperature at the vertex of the rille, which was assumed to have a symmetrical V-shape, was calculated from the solar input alone; for this geometry, the vertex sees neither wall. The temperature was assumed to vary linearly from the vertex to the top of the rille. The radiation-balance method resulted in a correction of 5 to 10 percent, and the vertex method resulted in a correction of 10 to 20 percent. The former value is considered to be the more reliable, mainly because the profile of the rille does not particularly resemble a V-shape. A correction of 10 percent is considered to be reasonably close to the upper limit of the effect that results from the cold rille wall.

The thermal effect of the Apennine Front was estimated in a preliminary way from the two-dimensional-slope method of Lachenbruch (ref. 11-19). By assuming two-dimensional symmetry, the curves given by Lachenbruch indicate that the correction, which is negative in this case, is 10 percent at a maximum. Actually, the heat-flow-experiment site is in an embayment in the Apennine Front, which invalidates the two-dimensional approximation and reduces the

correction. A correction of 5 percent would be more realistic.

In summary, the topographic effect of Hadley Rille is approximately canceled by the effect of the Apennine Front, which leaves only the cold-spot effect of the rille as a remaining correction resulting from the visible topography. This latter correction is the largest correction, in any case, and seems most likely to approximate 10 percent of the measured heat flow.

## Implications of the Results

In this section, the view was adopted that the heat flow observed at the Hadley Rille site is representative of the moonwide value, in spite of the possibilities of local and regional disturbances and large-scale variations in the lunar heat flow. Thus, the measurement is considered at face value, with full realization that future measurements may produce major changes in the conclusions. Because of the preliminary nature of the results, simple models were used for this report. Only the linear equation of heat conduction was considered, for which the thermal diffusivity was constant.

The value that is considered to be an upper limit to the heat flow resulting from the initial heat is calculated by assuming that, at the end of a convective stage in the early history of the Moon, temperatures throughout the Moon lay along the solidus for lunar basalt (ref. 11-20). After $3 \times 10^9$ yr, the heat flow resulting from these very high initial temperatures is in the range of $0.2 \times 10^{-6}$ to $0.4 \times 10^{-6}$ W/cm$^2$. If, as suggested by the greater ages of all known lunar rocks, partial melting throughout the Moon took place earlier, still lower values of heat flow would be associated with the initial heat. It is likely that the assumed initial temperatures are too high; however, by revising the assumed temperatures downward, the flux from the initial heat is further reduced. The initial heat contributes little to the present lunar heat flow, and the contribution can be neglected for present purposes.

The major portion of the heat flow from the Moon probably results from radioactive heat generation in the interior. It is possible to construct an infinite number of models based on nonuniform distributions of radioactivity; however, in this report, the discussion was confined to consideration of the Moon as a sphere with uniform and constant internal heat generation. The ratio of the surface heat flow $q$ (expressed in $10^{-6}$ W/cm$^2$) and the heat production $Q$ (expressed in $10^{-13}$ W/cm$^3$) is shown for several times in the following list.

| Time, yr | $q/Q$, cm |
|---|---|
| $3 \times 10^9$ | $3.22 \times 10^7$ |
| 4 | 3.58 |
| 5 | 3.89 |
| Infinite | 5.78 |

With a lunar heat flow of $3.3 \times 10^{-6}$ W/cm$^2$, the value of $Q$ must be in the range of $0.57 \times 10^{-13}$ to $1.0 \times 10^{-13}$ W/cm$^3$. This number is far lower than the heat production of lunar basalt, which has a value of approximately $3.5 \times 10^{-13}$ W/cm$^3$. However, the basaltic rocks are presumably differentiates that are far more radioactive than the parent material. On the other hand, ordinary chondrite and type I carbonaceous chondrites generate heat at rates of approximately $0.17 \times 10^{-13}$ and $0.22 \times 10^{-13}$ W/cm$^3$, respectively. The respective average rates of heat generation over the last $4.5 \times 10^9$ yr are $0.61 \times 10^{-13}$ and $0.67 \times 10^{-13}$ W/cm$^3$. Even these last figures are barely sufficient to provide the necessary flux. The conclusion is that, if the observed lunar heat flow originates from radioactivity, then the Moon must be more radioactive than the classes of meteorites that have formed the basis of Earth and Moon models in the past.

# APPENDIX

## Equilibration of an Infinitely Long Cylinder in a Homogeneous Medium by Conduction

In this appendix, the theory of the cooling of a cylinder by conduction is reviewed and applied to the heat-flow probe. Cylindrically shaped probes are commonly used in making geothermal measurements, and, as a consequence, the theory of heat flow in cylindrical coordinates has been thoroughly investigated (refs. 11-11, 11-14, and 11-21). The investigation of the effect of a finite contact resistance between a cylinder and the surrounding medium (ref. 11-14) is particularly applicable to problems of the cooling of the lunar probes. In this appendix, the solution (ref. 11-14) has been extended to a somewhat more complex model that includes a solid cylinder inside a thin-walled concentric cylinder which, in turn, is surrounded by an infinite medium with a conductivity $k$. The cylinders are assumed to be perfect conductors; that is, each cylinder is isothermal, which is very nearly true in the case of the heat-flow probe. Contact resistances exist at the two cylindrical boundaries. In this model, the inner cylinder is an idealization of the heat-flow probe, which is radiatively coupled to the borestem (the concentric cylinder). The borestem, in turn, loses heat by conduction to the surrounding regolith, of conductivity $k$, through a thin zone of lunar material that has been disturbed by drilling and, hence, has a different conductivity. The initial temperature of the surrounding infinite medium is zero; and, initially, the two inner cylinders have a temperature $v_0$.

By defining the dimensionless parameter $\tau$ as $\kappa t/b^2$ (where $\kappa$ is the thermal diffusivity of the surrounding infinite medium, $t$ is time in seconds, and $b$ is the radius of the outermost cylinder), the ratio of the inner-cylinder temperature $v(\tau)$ to the inner-cylinder initial temperature $v_0$ is given by

$$\frac{v(\tau)}{v_0} = \int_0^\infty \frac{(1 - Au^2)\exp(-u^2\tau)\,du}{u\left(\left\{u(1 - Au^2)J_0(u) - \left[hu^2(1 - Au^2) - \alpha(1 - Bu^2)\right]J_1(u)\right\}^2 + \left\{u(1 - Au^2)Y_0(u) - \left[hu^2(1 - Au^2) - \alpha(1 - Bu^2)\right]Y_1(u)\right\}^2\right)} \tag{11-12}$$

where

$\alpha = 2\pi b^2 \rho c/(S_1 + S_2)$
$h = k/bH_2$
$A = S_2\gamma\kappa/b^2(S_1 + S_2)$
$B = \gamma\kappa/b^2$
$\gamma = S_1/2\pi aH_1$
$a$ = radius of the inner cylinder (heat-flow probe) in centimeters
$b$ = outer radius of the concentric outer cylinder (borestem) in centimeters
$S_1, S_2$ = thermal heat capacities per unit length of the inner and outer cylinders, respectively, W-sec/cm-K
$H_1, H_2$ = contact conductances at the inner- and outer-cylinder boundaries, respectively, W/cm$^2$-K
$\rho$ = density of the surrounding material, g/cm$^3$
$c$ = heat capacity per unit mass of the surrounding material, W-sec/g-K
$k$ = thermal conductivity of the surrounding material, W/cm-K
$\kappa$ = thermal diffusivity ($k/\rho c$) of the surrounding material, cm$^2$/sec

Also, $J_0(u)$, $J_1(u)$, $Y_0(u)$, and $Y_1(u)$ are the zero- and first-order Bessel functions of the first and second kinds.

By following the method described in reference 11-11, the expression on the right-hand side of equation (11-12) can be redesignated $f(A,h,\alpha,\tau)$; therefore, equation (11-12) can be written as $v(\tau)/v_0 = f(A,h,\alpha,\tau)$. A more complete derivation of equation (11-12) and the resulting tabulated values will be published at a later date. Two typical plots of $f(A,h,\alpha,\tau)$ are shown in figure 11-8. The values of $k$

and $H_2$ that were used for computing the theoretical curves are given in table 11-II. Other parameters are $\alpha$ = 3.33, $H_1$ = 3.25 × $10^{-4}$ W/cm$^2$ - K, $\gamma$ = 445 sec, and $a$ and $b$ are 0.95 and 1.259 cm, respectively.

By using asymptotic values of the Bessel functions for large values of $\tau$ (after a method outlined in ref. 11-21), a solution that is valid for long times can be derived as follows.

$$\frac{(x,\tau)}{T_0} \quad \frac{1}{2\alpha\tau} \cdot \frac{1}{4\alpha^2\tau^2}\left\{4\pi k\left[\frac{2S_1 \cdot S_2}{(S_1 \cdot S_2)^2}\right] \cdot 4h \quad 2 \quad (\alpha \quad 2)\ln\left(\frac{1}{S}\right)\right\} \qquad (11\text{-}13)$$

where ln ($S$) = 0.5772 (Euler's constant). The long-term solution exhibits some interesting features of the function $f(A,h,\alpha,\tau)$. At long times ($\tau > 20$), the function becomes nearly equal to $(2\alpha\tau)^{-1}$, or $(4k\pi t/S_1 + S_2)^{-1}$, which is independent of $\rho c$. A log-log plot of $f(A,h,\alpha,\tau)$ is shown in figure 11-8; for long times, the function describes a straight line with a slope of very nearly −1. This property of the function enables the temperature histories to be extrapolated to equilibrium values by the procedure described in the text of this section and a value for $k$ to be determined independently of $\rho c$ from long-time portions of the equilibration curves. In addition, as shown by equation (11-13), the contact conductances $H_1$ and $H_2$, which are contained in the constants $\gamma$ and $h$, become less important with time (because they are multiplied by $t^{-2}$).

## REFERENCES


11-1. Wesselink, A.J.: Heat Conductivity and Nature of the Lunar Surface Material. Bull. of the Astron. Inst. Neth., vol. 10, 1948, pp. 351-363.

11-2. Birkebak, Richard C.; Cremers, Clifford J.; and Dawson, J.P.: Thermal Radiation Properties and Thermal Conductivity of Lunar Materials. Science, vol. 167, no. 3918, Jan. 30, 1970, pp. 724-726.

11-3. Watson, K.I.: Thermal Conductivity Measurements of Selected Silicate Powders in Vacuum from 150-350 K, II. An Interpretation of the Moon's Eclipse and Lunation Cooling Curve as Observed Through the Earth's Atmosphere from 8-14 Microns. Thesis, Calif. Inst. Technol., 1964.

11-4 Linsky, Jeffrey L.: Models of the Lunar Surface Including Temperature Dependent Thermal Properties. Icarus, vol. 5, 1966, pp. 606-634.

11-5. Lee, William H.K.; and Uyeda, Seiya: Review of Heat Flow Data. Terrestrial Heat Flow, ch. 6, William H.K. Lee, ed., Am. Geophys. Union of Nat'l. Acad. of Sci.-Nat'l Res. Council (Washington), 1965, pp. 87-190.

11-6. Baldwin, J.E.: Thermal Radiation from the Moon and the Heat Flow Through the Lunar Surface. Royal Astronomical Society Monthly Notice 122, 1961, pp. 513-522.

11-7. Troitskiy, V.S.; and Tikhonova, T.V.: Thermal Radiation from the Moon and the Physical Properties of Its Upper Mantle. NASA TT F-13455, 1971.

11-8. Fricker, Peter E.; Reynolds, Ray T.; and Summers, Audrey L.: On the Thermal History of the Moon. J. Geophys. Res., vol. 72, no. 10, May 15, 1967, pp. 2649-2663.

11-9. Cremers, C.J.; and Birkebak, R.C.: Thermal Conductivity of Fines from Apollo 12. Proceedings of the Second Lunar Science Conference, vol. 3, A.A. Levinson, ed., MIT Press (Cambridge, Mass.), 1971, pp. 211-216.

11-10. Robie, Richard A.; Hemingway, Bruce S.; and Wilson, William H.: Specific Heats of Lunar Surface Materials from 90 to 350 Degrees Kelvin. Science, vol. 167, no. 3918, Jan. 30, 1970, pp. 749-750.

11-11. Bullard, E.C.: The Flow of Heat Through the Floor of the Atlantic Ocean. Proc. Royal Soc. London, A, vol. 222, 1954, pp. 408-429.

11-12. Cremers, C.J.; Birkebak, R.C.; and White, J.E.: Lunar Surface Temperatures at Tranquility Base. AIAA paper 71-79, AIAA Ninth Aerospace Sciences Meeting (New York, N.Y.), Jan. 25-27, 1971.

11-13. Langseth, MD., Jr.; Drake, E.I.; and Nathanson, D.: Development of an In Situ Thermal Conductivity Measurement for the Lunar Heat Flow Experiment. Lunar Thermal Characteristics, John Luca, ed., AIAA Lunar Progress Series, 1971.

11-14. Jaeger, J.C.: Conduction of Heat in an Infinite Region Bounded Internally by a Circular Cylinder of a Perfect Conductor. Australian J. Phys., vol. 9, 1956, pp. 167-179.

11-15. Murray, Bruce C.; and Wildey, Robert L.: Surface Temperature Variations During the Lunar Nighttime. Astrophys. J., vol. 139, no. 2, Feb. 15, 1964, pp. 734-750.

11-16. Winter, D.F.; and Saari, J.M.: A Particulate Thermophysical Model of the Lunar Soil. Astrophys. J., vol. 156, no. 3, June 1969, pp. 1135-1151.

11-17. Birch, Francis: Flow of Heat in the Front Range, Colorado. Bull. Geol. Soc. Am., vol. 61, no. 6, June 1950, pp. 567-630.

11-18. Jaeger, J.C.; and Sass, J.H.: Lees's Topographic Correction in Heat Flow and the Geothermal Flux in Tasmania. Geofis. Pura Appl., vol. 54, 1962, pp. 53-63.

11-19. Lachenbruch, A.H.: Rapid Estimation of the Topographic Disturbance to Superficial Thermal Gradients. Rev. Geophys., vol. 6, no. 3, Aug. 1968, pp. 365-400.

11-20. Ringwood, A.E.; and Essene, E.: Petrogenesis of Apollo 11 Basalts, Internal Composition and Origin of the Moon. Proceedings of the Apollo 11 Lunar Science Conference, vol. 1, A.A. Levinson, ed., Pergamon Press (New York, 1970, pp. 769-799.

11-21. Blackwell, J.H.: A Transient-Flow Method for Determination of Thermal Constants of Insulating Materials in Bulk. J. Appl. Phys., vol. 25, 1955, pp. 137-144.

## ACKNOWLEDGMENTS

The authors wish to express their sincere appreciation to the many individuals whose enthusiasm and efforts have made possible the successful undertaking of this experiment. In particular, we wish to thank the personnel of the five corporations that developed, fabricated, and tested the essential instrumentation: Bendix Corporation of Ann Arbor, Michigan; Arthur D. Little, Inc., of Cambridge, Massachusetts; The Data Systems Division of Gulton Industries, Inc., of Albuquerque, New Mexico; Martin-Marietta Corporation of Denver, Colorado; and Rosemount Engineering Company of Minneapolis, Minnesota. The advice, encouragement, and active support of M. Ewing and the efforts of H. Gibbon, K. Peters, and R. Perry, all of the Lamont-Doherty Geological Observatory, were essential to the success of the program. The support of G. Simmons of the NASA Manned Spacecraft Center throughout the development of the experiment also is appreciated.